Journal of Power Sources 195 (2010) 3149–3154

Contents lists available at ScienceDirect

Journal of Power Sources

journal homepage: www.elsevier.com/locate/jpowsour

Short communication

Intermediate temperature fuel cell with a doped ceria–carbonate composite electrolyte

Chun Xia[a], Yi Li[b], Ye Tian[a], Qinghua Liu[a], Zhiming Wang[a], Lijun Jia[a], Yicheng Zhao[a], Yongdan Li[a,*]

[a] Tianjin Key Laboratory of Applied Catalysis Science and Technology and State Key Laboratory for Chemical Engineering (Tianjin University), School of Chemical Engineering, Tianjin University, Weijin Road 92, Tianjin 300072, China
[b] Chemistry Department, Tianjin University, Tianjin 300072, China

ARTICLE INFO

Article history:
Received 6 November 2009
Received in revised form
20 November 2009
Accepted 25 November 2009
Available online 1 December 2009

Keywords:
Ternary ionic conduction
Interfacial effect
Intermediate temperature fuel cell
Composite electrolyte
Molten carbonate
Samarium doped ceria

ABSTRACT

The performance of a composite electrolyte composed of a samarium doped ceria (SDC) and a binary eutectic carbonate melt phase has been examined. This material shows higher ionic conductivity than pure SDC in intermediate temperature region. SDC with different morphologies is obtained by co-precipitation, sol–gel and glycine-nitrate combustion preparation techniques. A tri-layer single cell is prepared with a cost-effective co-pressing and co-sintering technique. It is found that the surface properties of SDC and the electrolyte thickness have a great influence on the fuel cell performance. When the co-precipitated SDC is used as the electrolyte component and CO_2/O_2 gas mixture is adopted as the cathode oxidant gas, a fuel cell with an excellent performance is obtained, which has a peak power output of 1704 mW cm^{-2} at a current density of 3000 mA cm^{-2} at 650 °C. The influence of cathode atmosphere is examined with conductivity measurement and fuel cell performance test. The results support the concept of $O^{2-}/H^{+}/CO_3^{2-}$ ternary conduction.

1. Introduction

Conventional solid oxide fuel cell (SOFC) uses yttria stabilized zirconia (YSZ) as electrolyte and operates at high temperatures (800–1000 °C) to achieve a sufficient ionic conductivity [1]. However, there are many disadvantages of high temperature operation, such as insufficient long-term stability, high manufacture cost, and difficulty in materials selection. To develop a cost-effective and marketable intermediate temperature (IT) SOFC, much research effort has been focused on the exploration of novel electrolyte materials with high ionic conductivity in IT region (500–800 °C) [2].

In recent years, oxide ion conductor, such as doped zirconia, ceria and perovskite type oxide have been explored extensively; meanwhile, proton conductors is also of great interest for academia [3–6]. Various film-preparation techniques, such as slurry coating, screen printing and tape casting have been examined to limit the ohmic loss through reducing the thickness of the electrolyte layer [7–10]. These efforts accelerate the development of ITSOFCs. However, insufficient ionic conductivity, electronic conduction, poor stability and high manufacturing cost still limit the application of ITSOFCs. Recently, salt–ceria-composite electrolytes (SCCEs) are found to be binary ionic (O^{2-}/H^{+}) conductors with an overall ionic conductivity of around 0.1 S cm^{-1} at 600 °C in air [11]. In our previous work, when CO_2/O_2 gas mixture was used as the cathode gas instead of air, it showed a great enhancing effect. To understand this effect, an $O^{2-}/H^{+}/CO_3^{2-}$ ternary ionic conduction mechanism was proposed for the composite electrolyte [12]. In this work, Sm doped CeO_2 (SDC) and Li/Na carbonates are used to make up the composite electrolyte. The effects of the SDC morphology and structure are examined. The influence of cathode gas is discussed further to validate the concept of ternary ionic conduction in SCCE.

2. Experimental

2.1. Preparation of composite electrolyte

SDC powder with a composition $Ce_{0.8}Sm_{0.2}O_{1.9}$ was prepared by three methods: (A) glycine-nitrate combustion (GN), (B) oxalate-co-precipitation (OC) and (C) sol–gel process (SG) [13–15]. Li_2CO_3 and Na_2CO_3 with a mol ratio of 1:1 were mixed thoroughly by ball milling for 4 h and heated at 600 °C in air for 1 h to form a binary eutectic salt. The eutectic salt and SDC were mixed with a weight ratio of 3:7, and then ground with an agate mortar. The material was calcined at 650 °C in air for 1 h to form a composite electrolyte. The corresponding composite electrolytes are labeled

* Corresponding author. Tel.: +86 22 27405613; fax: +86 22 27405243.
E-mail address: ydli@tju.edu.cn (Y. Li).

0378-7753/$ – see front matter © 2009 Elsevier B.V. All rights reserved.
doi:10.1016/j.jpowsour.2009.11.104

as GNCE, OCCE and SGCE, respectively. The composite electrolyte powder was pressed at 300 MPa into a cylindrical pellet with a diameter of 13 mm and thickness of 1 mm using a uniaxial die-pressing technique. The green pellets were then sintered at 650 °C for 1 h. Silver electrodes were subsequently prepared by painting silver paste onto either sides of the pellet for conductivity test. The pellet was sintered at 700 °C for 4 h afterwards.

2.2. Characterization

The powder X-ray diffraction (XRD) patterns were recorded at room temperature using a D/max 2500 v/pc instrument (Rigaku Corp. Japan) with CuKα radiation, 40 kV and 200 mA. The morphology of powders and the microstructure of sintered pellets were observed with a PHILIPS XL 30 scanning electron microscope (SEM). The phase transition behavior of the composite was measured by PerkinElmer Diamond TG/DTA in air with a heating rate of 4 °C min^{-1}. Nitrogen adsorption/desorption experiments were performed with a Quantachrome Autosorb-1 analyzer at −196 °C. The specific surface area of each sample was calculated by the multiple points Brunauer–Emmett–Teller method. The electrical conductivity of the pellet was measured in air by A.C. impedance spectroscopy in a temperature range of 300–650 °C using an electrochemical workstation, CHI660B, made by Cheng Hua Corp. in China, in a frequency range from 1 Hz to 100 kHz with a bias voltage of 5 mV.

2.3. Fuel cell test

The anode material was a mixture of NiO (50 vol.%) and the SCCE (50 vol.%). The cathode was made with mixing the SCCE (50 vol.%) and the lithiated NiO powder (50 vol.%) prepared by solid-state reaction of LiOH and NiO at 700 °C for 3 h [16]. A tri-layer single cell structure was made by a modified co-pressing technique, see Fig. 1. (a) The anode support was formed first by a uniaxial die-pressing technique. The electrolyte was then fed as a layer of powder on the support with the aid of a 60 mesh sieve as shown in the figure. (b) With 30 MPa pressure applied, a thin layer of electrolyte was formed on the top of the support. (c) The cathode layer was formed on the top of the electrolyte in the same way. (d) The tri-layer pellet was finally pressed at 300 MPa. The green pellet was sintered at 650 °C for 1 h. The final pellet has a diameter of 13 mm. The thickness of the anode is 0.5 mm, while that of the cathode is 0.25 mm. The thickness of the electrolyte varied in order to investigate the effect of the thickness. The thickness of each layer was measured with an optical microscope. Silver paste was coated afterwards on each side to act as the current collector followed with 700 °C thermal treatment. A homemade setup was used for the performance measurement of the single cell. The fuel cell was tested in a temperature range of 450–650 °C under atmospheric pressure. Hydrogen and CO_2/O_2 (1:1 in vol.%) gas mixture were used as the fuel and oxidant, respectively. The gas flow rates in both sides were 100 ml min^{-1} (STP). The fuel cell *I–V* characteristics were measured by the SM-102 fuel cell tester made by San Mu Corp. China.

Table 1
Crystallite sizes in (1 1 1) direction of different SDC samples investigated.

Sample	GN	OC	SG
Crystal size (nm)	30.5	25.8	17.3

3. Results

3.1. Property of composite electrolyte

The powder XRD patterns of SDC prepared by the described techniques and the corresponding composite electrolytes are presented in Fig. 2. All the patterns show only the characteristics of the cubic fluorite phase, which is in good agreement with JCPDS file 34-394. The mean crystallite sizes of the SDC samples are listed in Table 1. The crystallite sizes of SDC are 30.5 nm, 25.8 nm and 17.3 nm for GN, OC and SG samples, respectively.

The SEM micrographs of the SDC powder prepared by the techniques described above are given in Fig. 3(a–c). The SDC (GN) presents a highly porous foam-like structure. SDC particles with a rod-like shape can be found in the SDC (OC) sample; whereas the SDC (SG) consists of aggregates with attachments and sintering. The SEM photos of the corresponding SCCE powders are shown in Fig. 3(d–f). It shows that the surfaces of the SDC particles are covered with amorphous carbonates. Clear interfaces in the OCCE and SGCE can be seen. For the GNCE, the foam-like morphology cannot

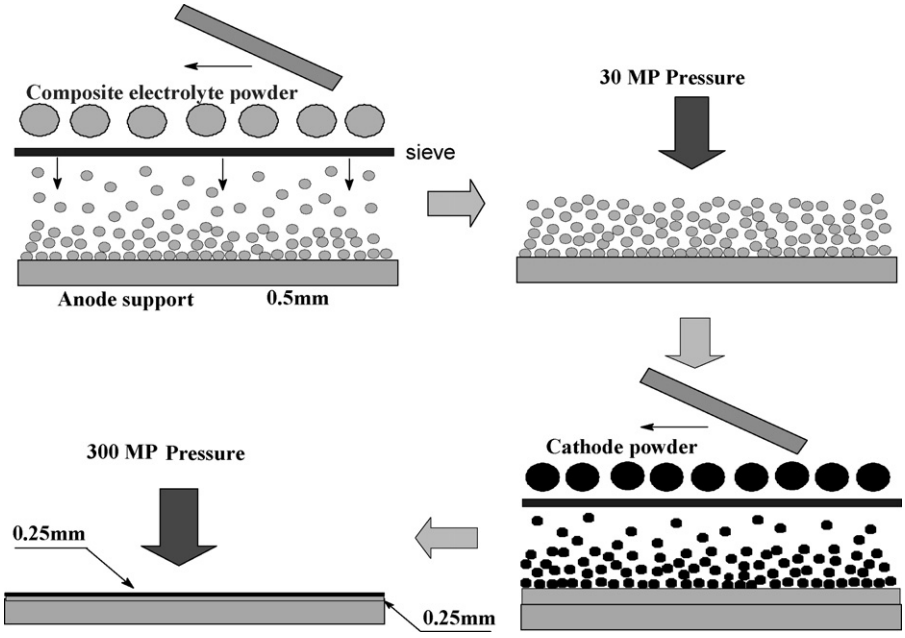

Fig. 1. The modified co-pressing process for tri-layer single cell.

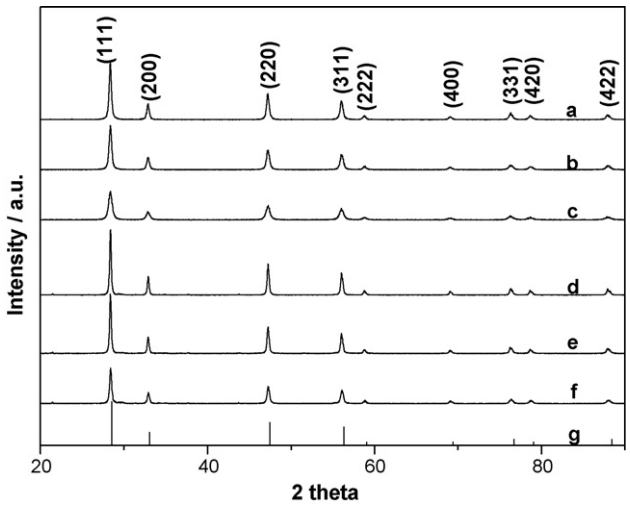

Fig. 2. XRD patterns of SDC prepared by different methods and corresponding composites. (a) GN; (b) OC; (c) SG; (d) GNCE; (e) OCCE; (f) SGCE; (g) JCPDS file 34-394.

Table 2
BET surface area of different SDC and SCCE investigated.

Sample	GN/GNCE	OC/OCCE	SG/SGCE
BET ($m^2\ g^{-1}$)	22.05/2.24	15.18/2.16	2.95/1.53

be distinguished, but a homogenous surface without a clear interface is observed. The BET surface area of SDC and their composites are listed in Table 2. The SDC (GN) has the highest surface area, 22.5 $m^2\ g^{-1}$; whereas SDC (SG) has the lowest surface area, only 2.9 $m^2\ g^{-1}$. After incorporation of carbonates, the surface areas of the three samples are all lower than 2.3 $m^2\ g^{-1}$.

The cross-sections of the SCCE pellets after sintering at 650 °C are presented in Fig. 4. It is interesting to note that the morphology of SCCEs in the pellets is different from those in the powders. The GNCE presents a porous structure without clear interface, whereas the consecutive interfaces can be observed clearly in OCCE. In SGCE, the SDC aggregates are covered by a carbonate layer showing a core–shell structure. The DTA curves of the SCCEs are depicted in Fig. 5. Each curve has only one endothermic event attributed to the melting of the eutectic salt in the temperature range of 450–500 °C. There exist slight shifts in the peak positions between the three

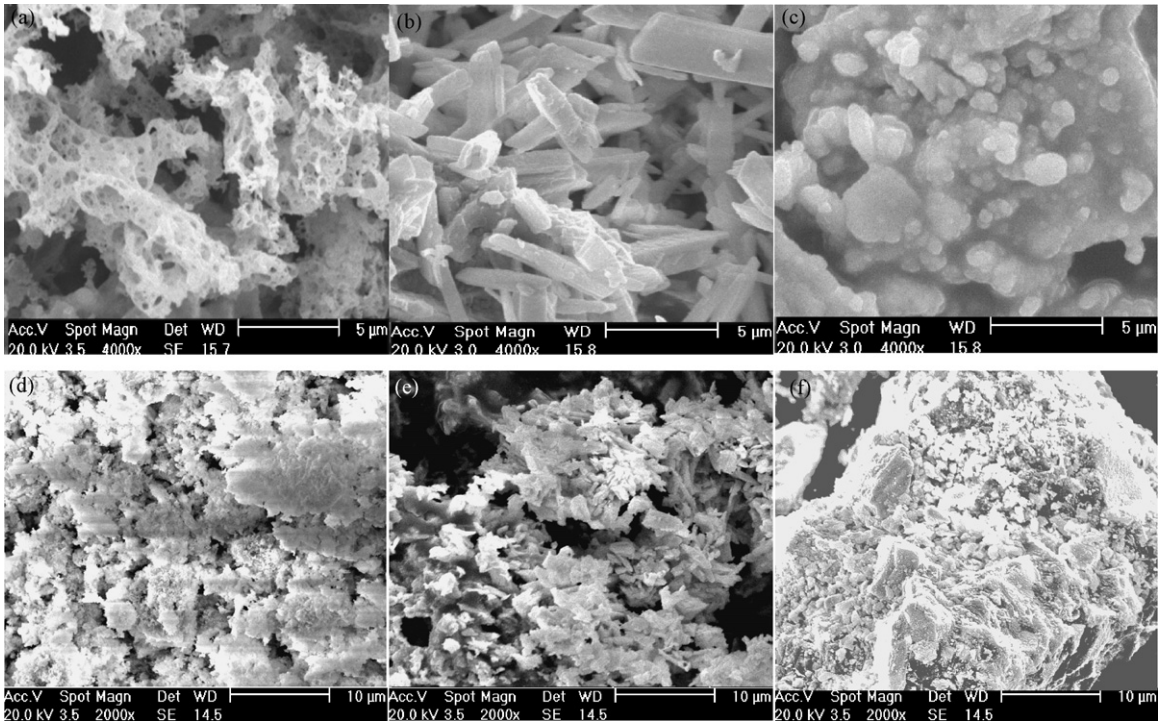

Fig. 3. SEM images of SDC powder prepared by various methods and their composites. (a) GN; (b) OC; (c) SG; (d) GNCE; (e) OCCE; (f) SGCE.

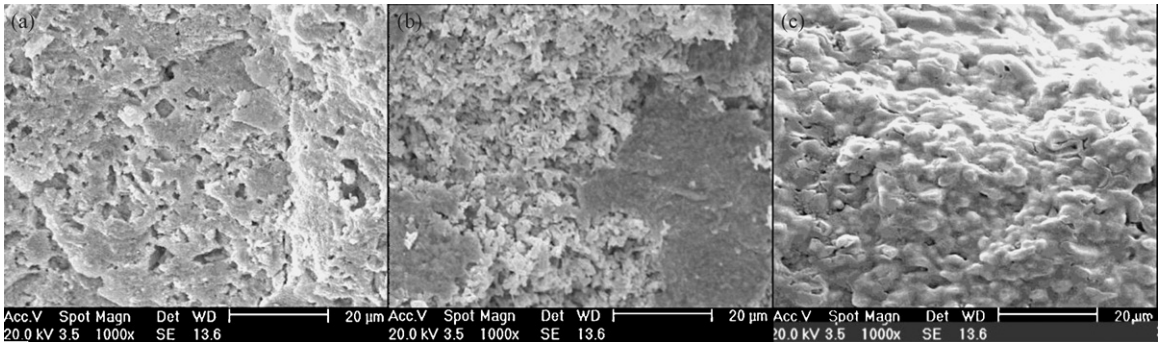

Fig. 4. SEM images of cross-section of composite electrolyte pellet sintered at 650 °C. (a) GNCE; (b) OCCE; (c) SGCE.

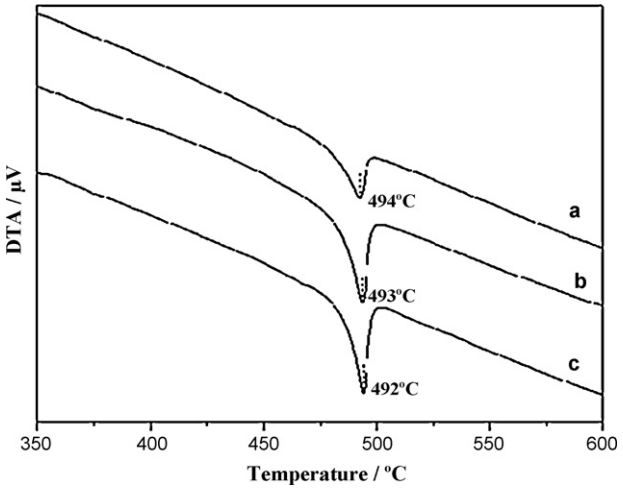

Fig. 5. DTA curves of composite electrolytes. (a) SGCE; (b) OCCE; (c) GNCE.

samples. The peak temperatures of the three curves locate at 492, 493 and 494 °C for SGCE, OCCE and GNCE, respectively.

The conductivity measured by the A.C. (CMAC) impedance technique versus temperature curves of the SDC and SCCE samples are plotted in Fig. 6. CMAC values of the SDC sample vary from 10^{-5} to 10^{-2} S cm^{-1} in the temperature range of 300–650 °C, while those of the SCCE samples vary from 10^{-4} to 10^{-1} S cm^{-1} in the same temperature range. The CMAC values of the SCCEs are around 1 order of magnitude higher than that of the SDC sample. The CMAC values of composite electrolyte above melting point appear in the order: SGCE > OCCE > GNCE.

3.2. Tri-layer and the performance of single cell

I–V and *I–P* curves at 650 °C with a 0.5 mm thick SCCE and with the CO_2/O_2 gas mixture as the oxidant are illustrated in Fig. 7. Here, the maximum output power densities of the single cells are 1266, 1121 and 607 mW cm^{-2} for OCCE, SGCE and GNCE as the electrolyte, respectively. Single cell with OCCE shows the best performance. Fig. 8 gives the *I–V–P* characteristics of the single cell measured with 0.25 mm thick OCCE electrolyte as a function of temperature. The open-circuit voltages (OCV) are 1.13, 1.10, 1.10, 1.07 and 1.06 V at 650, 600, 550, 500, and 450 °C, respectively. The maximum output appeared at 650 °C and reached 1704 mW cm^{-2} at a current density of 3000 mA cm^{-2}. It should be noted that, after the fuel cell was operated for 30 min, water was condensed in both outlet gas streams and CO_2 was detected by GC in the anode outlet gas.

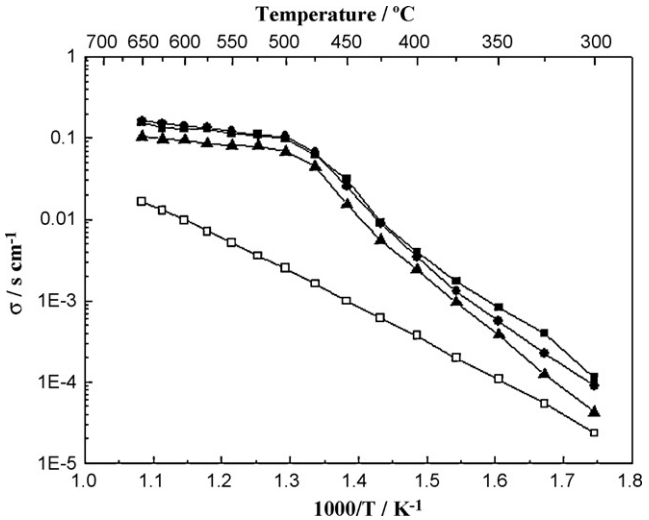

Fig. 6. The conductivity measured by impedance technique of different electrolytes. (●) SGCE; (■) OCCE; (▲) GNCE; (□) SDC.

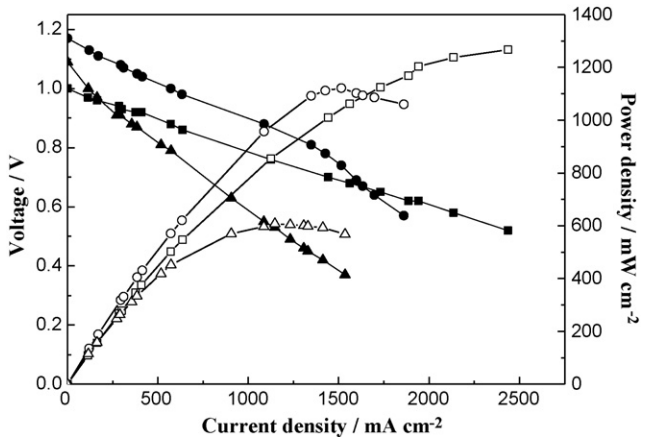

Fig. 7. Performances of H_2/O_2–CO_2 single cell with different composite electrolytes (0.5 mm) at 650 °C. (●, ○) SGCE; (■, □) OCCE; (▲, △) GNCE.

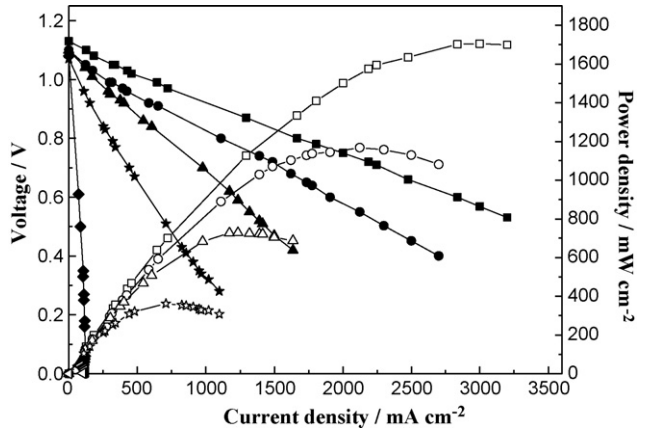

Fig. 8. Performance of single cell with 0.25 mm thickness OCCE at different temperatures in H_2/O_2–CO_2 atmosphere. (■, □) 650 °C; (●, ○) 600 °C; (▲, △) 550 °C; (★, ☆) 500 °C; (♦, ◊) 450 °C.

The influence of cathode gas on the OCV and the maximum power density of a single cell in air and CO_2/O_2 are compared in Fig. 9. Above the melting point (493 °C), the fuel cell shows higher

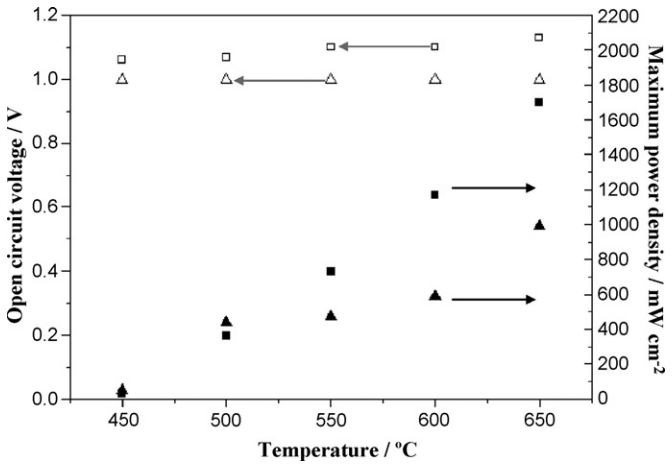

Fig. 9. The influence of cathode gas on the OCV and maximum power density with OCCE in air and O_2–CO_2 mixed gas, (■, □) O_2–CO_2 mixed gas, and (▲, △) air.

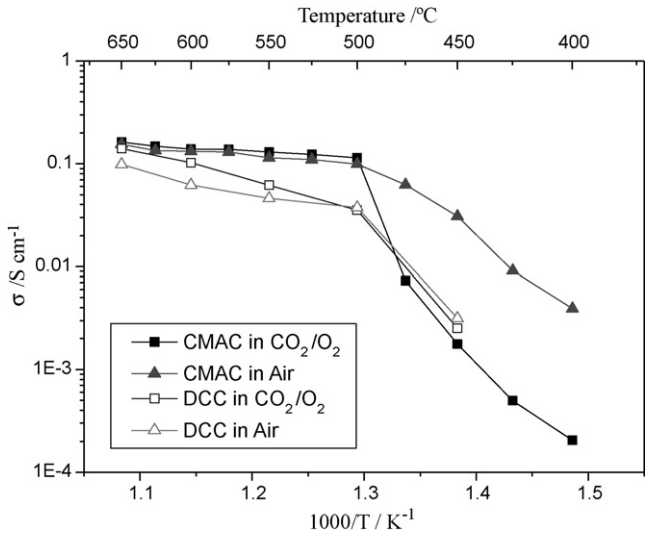

Fig. 10. The conductivity measured by A.C. (CMAC) impedance technique and D.C. conductivity (DCC) results of OCCE in different cathode gases as a function of temperature. (■, □) O_2–CO_2 mixed gas and (▲, △) air.

power output with CO_2/O_2 mixed gas than with air, whereas, below the melting point, air is more favored. The single cell with the same component shows higher OCV with mixed gas than with air. For the *V*–*I* characteristics in Fig. 8, the linear section in the central region reflects the internal resistance (IR) loss caused mainly by electrolyte, from which the resistance and thus D.C. conductivity (DCC) of the electrolyte can be calculated [17]. The DCC and CMAC of OCCE with air and mixed gas are compared in Fig. 10. The CMAC of OCCE is higher than its DCC, while the DCC gets closer to the CMAC with the increase of temperature. Both the CMAC and DCC with mixed gas are higher than those with air, whereas it shows the opposite trend below the melting point.

4. Discussion

4.1. Fabrication of a single cell

The ohmic loss of the electrolyte layer can be suppressed by reducing its thickness [18]. To achieve the goal, several wet film-preparation techniques such as screen printing and slurry coating have been explored. The anode has been usually used as the support simultaneously, on which the thin electrolyte and cathode layers are coated, respectively. For the conventional yttria stabilized zirconia (YSZ) electrolyte, Ni/YSZ anode and $La_xSr_{1-x}MnO_{3-\delta}$/YSZ cathode, heat treatment above 1300 °C has been applied after each coating for the densification of the electrolyte and improvement of the contact between layers. These techniques based on wet and high temperature treating processes are generally cost intensive, and also introduce polarization losses due to the high temperature destruction of the electrode microstructures. Such techniques often employ organic additives which pollute the environment. Here, we introduce a modified dry pressing technique without using organic additives. Different from previous literature, a fragmentation and filling process with the aid of a sieve were employed. This technique helps to fabricate the electrolyte and the cathode layers as thin as 250 μm, while in literature normally 500 μm was obtained for the two layers with a co-pressing technique [19,20]. The tri-layer structure was prepared by one step co-pressing process, which was superior to the multistep coating processes. The molten carbonate fills in the pores of SDC matrix thus forms a gas-tight electrolyte layer. This is proved by the high OCV (>1 V) in Fig. 8. Molten carbonate simultaneously improves the contact between electrodes and electrolyte which limit the contact resistance. The low calcination temperature of the materials protects the porous structure of the electrodes which facilitates gas diffusion and minimizes polarization losses.

4.2. The composite electrolyte

The XRD patterns of all the SDC samples examined show a similar pure and well crystallized fluorite structure. However, the three preparation techniques produced SDC with distinctly different surface properties. In GN process, the combustion of the organic additive results in a production of gas and a porous structure with a large specific surface area [21]. OC technique produces perfect crystals with moderate surface area, while the aggregation of fine particles in SG route gives the smallest surface area among the three samples.

After incorporation of the carbonate, the composite electrolytes show an exactly same diffraction pattern as that of the pure SDC, and there are no diffraction peaks of carbonates, indicating that the carbonates exist in an amorphous form. This was also reported by other authors [22]. The DTA peak position and the CMAC values of the three composite materials show a same order: SG > OC > GN which indicates some dependence of the property of the composite on the structure of the SDC substrates. The structure of the solid oxide phase influences the thermal and ionic conduction property of the molten carbonate. Such effects has been found in many molten salts, such as alkali nitrates [23], and alkali binary carbonate [24], coexisting with oxide powders such as $LiAlO_2$, ZrO_2, MgO, Al_2O_3, and SiO_2 [23–26]. This has been explained as the interfacial effect or interaction between the two phases. It has been demonstrated that the ionic conduction within dual-phase composites depends on the quantity, distribution, and structure of the solid matrix. The high surface area oxide phase presents a tortuous path for both ionic conduction and diffusion in the dual-phase material, which often has a negative effect [25]. The endothermic peak in DTA shifts toward lower temperatures with the increase of the specific surface area of the solid oxide particles. It should be noted that most of the solid substrates reported are insulators. However, in this work, an ionic conductor, SDC, is employed as the solid matrix. The foam-like GN with the highest BET surface area shows the lowest CMAC and endothermic peak temperature of GNCE. On the other hand, SG with lowest BET surface area has the highest CMAC and endothermic peak temperature of SGCE. These results demonstrate that the solid ionic conductors have the same influences on the thermal and conductive properties of composite materials as the insulators.

From Fig. 7, it is found that the single cell with OCCE shows the best performance, which has a maximum power output of 1266 mW cm^{-2} at 2.4 A cm^{-2}. Compared to the results of CMAC, it seems that there is some conflict. However, it should be noted that all the ions, e.g. M^+ (M = Li, Na), CO_3^{2-} and O^{2-} in SCCE contribute to the CMAC [27]. The Li^+/Na^+ cations are non-consumed-supplied mobile ions and are blocked in fuel cell operation atmosphere. In order to get the sense of the effective conductivity, the DCC value is obtained through direct measurement of the fuel cell *I*–*V* characteristics [17]. The contribution of the mobile ions (H^+, O^{2-} and CO_3^{2-}) in H_2/CO_2–O_2 atmosphere can be characterized directly by the DCC. The DCC of OCCE, SGCE and GNCE are 0.13, 0.10 and 0.06 S cm^{-1} at 650 °C, respectively, which is consistent with the trend of fuel cell performances. The difference can be attributed to the influence of SDC structure on the interfacial effect [28]. In previously published works, many facts proved that the interfacial conduction in SCCE is the dominant process [29,30]. The fuel cell performance is greatly improved by increasing the interfacial area. It was found that a high interface area and consecutive dual-phase structure are crucial to the interfacial ionic conduction [31]. Here, the foam-like SDC (GN)

may distort the interfacial conduction path and limit the continuity of the molten carbonate phase [28]. For SDC (SG), the aggregation destroys the consecutive phase of SDC, which decreases the interfacial conduction area. The SDC (OC) sample shows perfect crystals with moderate specific surface area. In Fig. 4(c), the consecutive interface can be observed clearly in OCCE. The incorporation of 30 wt% carbonate makes the two phases have similar volume and maximizes the interface area and keeps the consecutive structure of each phase in the composite material [12].

When the thickness of OCCE layer is decreased to 250 μm, the maximum power density of single cell is 1704 mW cm^{-2} at a current density of 3 A cm^{-2}. The fuel cell shows a high OCV (>1.06 V), which proves the gas-tight structure of OCCE and free of electron conduction. This excellent and reproducible performance is attributed to super-ionic conduction and compatible electrodes. Recently, Li and Sun tested the stability of the H_2/CO_2–O_2 fuel cell with SCCE for 200 h [32]. A stable OCV and *V*–*I* performance was reported.

The influence of cathode atmosphere on fuel cell and SCCE was demonstrated in Figs. 9 and 10. The OCV with mixed gas is higher than with air, which is supposed to be the effect of the CO_2 and O_2 partial pressures. The single cell exports higher power density with mixed gas than with air above the melting point, while air as the cathode gas gives better result below the melting point. This is consistent with the results of CMAC and DCC measurements as shown in Fig. 10. When air is used as the cathode gas, H^+/O^{2-} binary conduction happens along the interface and in SDC phase, which has already been proved by electrolysis of water, gas concentration cells and fuel cell studies [17,33]. However, the conduction of CO_3^{2-} is blocked in these cases because of no external resource for CO_3^{2-}. When CO_2–O_2 mixture is used, higher power density, CMAC and DCC of SCCE is obtained compared with air. CO_2 in cathode gas may stimulate the CO_3^{2-} conduction in molten carbonate bulk phase as in molten carbonate fuel cell and promote H^+/O^{2-} conduction by interaction between ions along the interface [34,35]. Recently, the promotion effect of CO_3^{2-} on O^{2-} conduction in solid inorganic membranes was elaborated both with experiments and theoretical modeling [36,37]. The ternary ionic conduction hypothesis is also consistent with the experiment fact that water was condensed in the outlet gas of cathode and anode and CO_2 was detected by GC in the anode outlet gas. Above the melting point, with the increase of temperature, the DCC of SCCE gets closer to the CMAC which is due to the increase of the ternary $O^{2-}/H^+/CO_3^{2-}$ conduction. However, below the melting point, the freezing of carbonate limits the carbonate conduction, and leads to the poor CMAC and DCC of SCCE and fuel cell performance.

5. Conclusion

A composite electrolyte based on SDC and $(Li/Na)_2CO_3$ eutectic salt was used as the electrolyte for the intermediate temperature fuel cell. This material has a much higher ionic conductivity than pure SDC in the temperature range higher than the melting point of the carbonate phase. Three techniques, i.e. glycine-nitrate combustion (GN), oxalate-co-precipitation (OC) and sol–gel method (SG) were employed in the synthesis of SDC with different morphologies. It was found that the SDC prepared with different method has different surface property which decides the thermal and ionic transport behavior of SCCE. The OCCE with rod-like SDC particle shows the best performance which has a moderate crystallite size and surface area. It favors the formation of consecutive interface and dual-phase for the ionic conduction.

A co-pressing and co-sintering process is employed to prepare the single cell. With such a cost-effective fabrication process, the performance of the single cell is greatly improved by decreasing the thickness of SCCE layer. When CO_2/O_2 gas mixture was used as the cathode oxidant gas, the single cell with OCCE exhibits an excellent performance with a peak power output of 1700 mW cm^{-2} at a current density of 3000 mA cm^{-2} at 650 °C. The CMAC, DCC of SCCE and fuel cell performance prove the enhancing effect of CO_2 which stimulates the CO_3^{2-} conduction and promotes the conduction of other mobile ions. Such intermediate temperature fuel cell with SCCE has the combination of the good features of SOFC/MCFC and is very promising for further research.

Acknowledgements

This work has been supported by the Natural Science Foundation of China under contract numbers 20425619 and 20736007. The work has also been supported by the Program of Introducing Talents to the University Disciplines under file number B06006, and the Program for Changjiang Scholars and Innovative Research Teams in Universities under file number IRT 0641.

References

[1] S.M. Haile, Acta Mater. 51 (2003) 5981–6000.
[2] B. Zhu, Int. J. Energy Res. 30 (2006) 895–903.
[3] Z.G. Lv, P. Yao, R.S. Guo, F.Y. Dai, Mater. Sci. Eng. A 458 (2007) 355–360.
[4] L. Minervini, M.O. Zacate, R.W. Grimes, Solid State Ionics 116 (1999) 339–349.
[5] D. Lee, J.H. Han, Y. Chun, R.H. Song, D.R. Shin, J. Power Sources 166 (2007) 35–40.
[6] H. Yokokawa, T. Horita, N. Sakai, K. Yamaji, M.E. Brito, Y.P. Xiong, H. Kishimoto, Solid State Ionics 174 (2004) 205–221.
[7] Y.J. Leng, S.H. Chan, K.A. Khor, S.P. Jiang, P. Cheang, J. Power Sources 117 (2003) 26–34.
[8] R. Hui, Z. Wang, S. Yick, R. Maric, D. Ghosh, J. Power Sources 172 (2007) 840–844.
[9] R. Peng, C. Xia, Xi. Liu, D. Peng, G. Meng, Solid State Ionics 152–153 (2002) 561–565.
[10] S.D. Kim, S.H. Hyun, J. Moon, J.H. Kim, R.H. Song, J. Power Sources 139 (2005) 67–72.
[11] B. Zhu, M.D. Mat, Int. J. Electrochem. Sci. 1 (2006) 383–402.
[12] C. Xia, Y. Li, Y. Tian, Q.H. Liu, Y.C. Zhao, L.J. Jia, Y.D. Li, J. Power Sources 188 (2009) 156–162.
[13] N. Ai, Z. Lu, K. Chen, X. Huang, Y. Liu, R. Wang, W. Su, J. Membr. Sci. 286 (2006) 255–259.
[14] R.S. Torrens, N.M. Sammes, G.A. Tompsett, Solid State Ionics 111 (1998) 9–15.
[15] W. Huang, P. Shuk, M. Greenblatt, Solid State Ionics 100 (1997) 23–27.
[16] J.B. Huang, L.Z. Yang, R.F. Gao, Z.Q. Mao, C. Wang, Electrochem. Commun. 8 (2006) 785–789.
[17] B. Zhu, Electrochem. Commun. 1 (1999) 242–246.
[18] J. Will, A. Mitterdorfer, C. Kleinlogel, D. Perednis, L.J. Gauckler, Solid State Ionics 131 (2000) 79–96.
[19] C. Jiang, J. Ma, X. Liu, G. Meng, J. Power Sources 165 (2007) 134–137.
[20] C.R. Xia, M. Liu, J. Am. Ceram. Soc. 84 (2001) 1903–1905.
[21] K. Singh, S.A. Acharya, S.S. Bhoga, Ionics 13 (2007) 429–434.
[22] J.B. Huang, Z.Q. Mao, L.Z. Yang, R.R. Peng, Electrochem. Solid State Lett. 8 (9) (2005) A437–A440.
[23] A.B. Béléké, M. Mizuhata, S. Deki, Vib. Spectrosc. 40 (2006) 66–79.
[24] M. Mizuhata, Y. Harada, G.J. Cha, A.B. Béléké, S. Deki, J. Electrochem. Soc. 151 (5) (2004) E179–E185.
[25] F.M. Delnick, R.A. Guidotti, J. Electrochem. Soc. 137 (1990) 11–16.
[26] M. Mizuhata, A.B. Béléké, H. Watanabe, Y. Harada, S. Deki, Electrochim. Acta 53 (2007) 71–78.
[27] J.B. Huang, Z.Q. Mao, Z.X. Liu, C. Wang, Electrochem. Commun. 9 (2007) 2601–2605.
[28] J.B. Huang, Z.Q. Mao, Z.X. Liu, C. Wang, J. Power Sources 175 (2008) 238–243.
[29] S. Li, X.D. Wang, B. Zhu, Electrochem. Commun. 9 (2007) 2863–2866.
[30] X.R. Liu, B. Zhu, J. Xu, J.C. Sun, Z.Q. Mao, Key Eng. Mater. 280–283 (2005) 425–430.
[31] B. Zhu, S. Li, B.E. Mellander, Electrochem. Commun. 10 (2008) 302–305.
[32] S. Li, J.C. Sun, Int. J. Hydrogen Energy (2009), doi:10.1016/j.ijhydene.2009.05.096.
[33] W. Zhu, C.R. Xia, D. Ding, X.Y. Shi, G.Y. Meng, Mater. Res. Bull. 41 (2006) 2057–2064.
[34] Q.H. Liu, Y. Tian, C. Xia, L.T. Thompson, B. Liang, Y.D. Li, J. Power Sources 185 (2008) 1022–1029.
[35] B. Zhu, X.R. Liu, Z.G. Zhu, R. Ljungberg, Int. J. Hydrogen Energy 33 (2008) 3385–3392.
[36] Z.B. Rui, M. Anderson, Y.S. Lin, Y.D. Li, J. Membr. Sci. 345 (2009) 110–118.
[37] Y.D. Li, Z.B. Rui, C. Xia, M. Anderson, Y.S. Lin, Catal. Today 148 (2009) 303–309.